within space-group-forbidden reflections. Departure from Friedel's law in electron diffraction was first noted experimentally by Miyake & Uyeda (1950). The prediction of space-group-forbidden bands (within space-group-forbidden reflections) by Cowley & Moodie (1959), on the other hand, was one of the first successes of *N*-beam theory. A detailed explanation was later given by Gjønnes & Moodie (1965). These are known variously as 'GM' bands (Tanaka *et al.*, 1983), or more simply and definitively as 'GS' (glide–screw) bands (this section). These extinctions have a close parallel with space-group extinctions in X-ray diffraction, with the reservation that only screw axes of order two are accurately extinctive under *N*-beam conditions. This arises from the property that only those operations which lead to identical *projections* of the asymmetric unit can have *N*-beam dynamical symmetries (Cowley *et al.*, 1961).

Additionally, CBED from perfect crystals produces high-order defect lines in the zero-order pattern, analogous to the defect Kikuchi lines of inelastic scattering, which provide a sensitive measurement of unit-cell parameters (Jones *et al.*, 1977; Fraser *et al.*, 1985; Tanaka & Terauchi, 1985).

The significant differences between X-ray and electron diffraction, which may be exploited in analysis, arise as a consequence of a much stronger interaction in the case of electrons (Section 2.5.2). Hence, thin, approximately parallel-sided crystal regions must be used in high-energy (100 kV–1 MV) electron transmission work, so that diffraction is produced from crystals effectively infinitely periodic in only two dimensions, leading to the relaxation of three-dimensional diffraction conditions known as 'excitation error' (Chapter 5.2). Also, there is the ability in CBED to obtain data from microscopic crystal regions of around 50 Å in diameter, with corresponding exposure times of several seconds, allowing a survey of a material to be carried out in a relatively short time.

In contrast, single-crystal X-ray diffraction provides much more limited symmetry information in a direct fashion [although statistical analysis of intensities (Wilson, 1949) will considerably supplement this information], but correspondingly gives much more direct three-dimensional geometric data, including the determination of unit-cell parameters and three-dimensional extinctions.

The relative strengths and weaknesses of the two techniques make it useful where possible to collect both convergent-beam and X-ray single-crystal data in a combined study. However, all parameters *can* be obtained from convergent-beam and electron-diffraction data, even if in a somewhat less direct form, making possible space-group determination from microscopic crystals and microscopic regions of polygranular material. Several reviews of the subject are available (Tanaka, 1994; Steeds & Vincent, 1983; Steeds, 1979). In addition, an atlas of characteristic CBED patterns for direct phase identification of metal alloys has been published (Mansfield, 1984), and it is likely that this type of procedure, allowing *N*-beam analysis by comparison with standard simulations, will be expanded in the near future.

2.5.3.1.2. *Zone-axis patterns from CBED*

Symmetry analysis is necessarily tied to examination of patterns near relevant zone axes, since the most intense *N*-beam interaction occurs amongst the zero-layer zone-axis reflections, with in addition a limited degree of upper-layer (higher-order Laue zone) interaction. There will generally be several useful zone axes accessible for a given parallel-sided single crystal, with the regions between axes being of little use for symmetry analysis. Only one such zone axis can be parallel to a crystal surface normal, and a microcrystal is usually chosen at least initially to have this as the principal symmetry axis. Other zone axes from that crystal may suffer mild symmetry degradation because the *N*-beam lattice component ('excitation error' extension) will not have the symmetry of the structure (Goodman, 1974; Eades *et al.*, 1983).

Upper-layer interactions, responsible for imparting three-dimensional information to the zero layer, are of two types: the first arising from 'overlap' of dynamic shape transforms and causing smoothly varying modulations of the zero-layer reflections, and the second, caused by direct interactions with the upper-layer, or higher-order Laue zone lines, leading to a sharply defined fine-line structure. These latter interactions are especially useful in increasing the accuracy of space-group determination (Tanaka *et al.*, 1983), and may be enhanced by the use of low-temperature specimen stages. The presence of these defect lines in convergent-beam discs, occurring especially in low-symmetry zone-axis patterns, allows symmetry elements to be related to the three-dimensional structure (Section 2.5.3.5; Fig. 2.5.3.4*c*).

To the extent that such three-dimensional effects can be ignored or are absent in the zero-layer pattern the *projection approximation* (Chapter 5.2) can be applied. This situation most commonly occurs in zone-axis patterns taken from relatively thin crystals and provides a useful starting point for many analyses, by identifying the projected symmetry.

2.5.3.2. *Background theory and analytical approach*

2.5.3.2.1. *Direct and reciprocity symmetries: types I and II*

Convergent-beam diffraction symmetries are those of Schrödinger's equation, *i.e.* of crystal potential, plus the diffracting electron. The appropriate equation is given in Section 2.5.2 [equation (2.5.2.6)] and Chapter 5.2 [equation (5.2.2.1)] in terms of the real-space wavefunction ψ. The symmetry elements of the crystal responsible for generating pattern symmetries may be conveniently classified as of two types (I and II) as follows.

I. The *direct* (type I: Table 2.5.3.1) symmetries imposed by this equation on the transmitted wavefunction given *z*-axis illumination ($\mathbf{k}_0$, the incident wavevector parallel to *Z*, the surface normal) are just the symmetries of φ whose operation leaves both crystal and *z* axis unchanged. These are also called 'vertical' symmetry elements, since they contain *Z*. These symmetries apply equally in real and reciprocal space, since the operator ∇^2 has circular symmetry in both spaces and does nothing to degrade the symmetry in

Table 2.5.3.1. *Listing of the symmetry elements relating to CBED patterns under the classifications of 'vertical' (I), 'horizontal' (II) and combined or roto-inversionary axes*

I. Vertical symmetry elements		
	International symbols	
	$2, 3, 4, 6$ $(2_1, 3_1, \ldots)$	
	m (c)	
	a, b (n)	
II. Horizontal symmetry elements		
	Diperiodic symbols	BESR symbols
	$2'$	m
	$2'_1$	
	m'	1_R
	a', b', n'	
	$\bar{1}'$	2_R
I + II	$\bar{4}'$	4_R
I × II	$\bar{3}' = 3 \times \bar{1}'$	$6_R = 3 \cdot 2_R$
	$\bar{6}' = 3 \times m'$	31_R

transmission. Hence, for high-symmetry crystals (zone axis parallel to z axis), and to a greater or lesser degree for crystals of a more general morphology, these zone-axis symmetries apply both to electron-microscope lattice images and to convergent-beam patterns under z-axis-symmetrical illumination, and so impact also on space-group determination by means of high-resolution electron microscopy (HREM). In CBED, these elements lead to *whole pattern* symmetries, to which every point in the pattern contributes, regardless of diffraction order and Laue zone (encompassing ZOLZ and HOLZ reflections).

II. Reciprocity-induced symmetries, on the other hand, depend upon ray paths and path reversal, and in the present context have relevance only to the diffraction pattern. Crystal-inverting or horizontal crystal symmetry elements combine with reciprocity to yield *indirect* pattern symmetries lacking a one-to-one real-space correspondence, within individual diffraction discs or between disc pairs. Type II elements are assumed to lie on the central plane of the crystal, midway between surfaces, as symmetry operators; this assumption amounts to a 'central plane' approximation, which has a very general validity in space-group-determination work (Goodman, 1984*a*).

A minimal summary of basic theoretical points, otherwise found in Chapter 5.2 and numerous referenced articles, is given here.

For a specific zero-layer diffraction order $g\ (= h, k)$ the incident and diffracted vectors are $\mathbf{k}_0$ and $\mathbf{k}_g$. Then the three-dimensional vector $\mathbf{K}_{0g} = \frac{1}{2}(\mathbf{k}_0 + \mathbf{k}_g)$ has the pattern-space projection, $\mathbf{K}_g = {}^{p}[\mathbf{K}_{0g}]$. The point $\mathbf{K}_g = \mathbf{0}$ gives the *symmetrical Bragg condition* for the associated diffraction disc, and $\mathbf{K}_g \neq \mathbf{0}$ is identifiable with the angular deviation of $\mathbf{K}_{0g}$ from the vertical z axis in three-dimensional space (see Fig. 2.5.3.1). $\mathbf{K}_g = \mathbf{0}$ also defines the symmetry centre within the two-dimensional disc diagram (Fig. 2.5.3.2); namely, the intersection of the lines S and G, given by the trace of excitation error, $\mathbf{K}_g = \mathbf{0}$, and the perpendicular line directed towards the reciprocal-space origin, respectively. To be definitive it is necessary to index diffracted amplitudes relating to a fixed crystal thickness and wavelength, with both crystallographic and momentum coordinates, as $\mathbf{u}_{g,K}$, to handle the continuous variation of $\mathbf{u}_g$ (for a particular diffraction order), with angles of incidence as determined by $\mathbf{k}_0$, and registered in the diffraction plane as the projection of $\mathbf{K}_{0g}$.

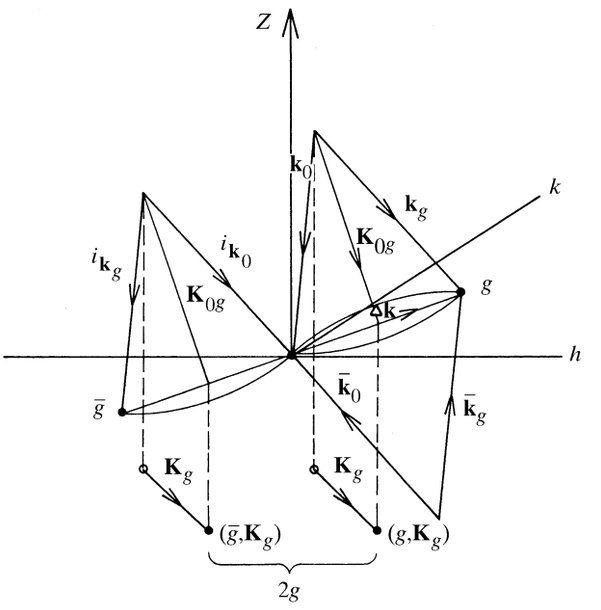

Fig. 2.5.3.1. Vector diagram in semi-reciprocal space, using Ewald-sphere constructions to show the 'incident', 'reciprocity' and 'reciprocity × centrosymmetry' sets of vectors. Dashed lines connect the full vectors $\mathbf{K}_{0g}$ to their projections $\mathbf{K}_g$ in the plane of observation.

2.5.3.2.2. *Reciprocity and Friedel's law*

Reciprocity was introduced into the subject of electron diffraction in stages, the essential theoretical basis, through Schrödinger's equation, being given by Bilhorn *et al.* (1964), and the N-beam diffraction applications being derived successively by von Laue (1935), Cowley (1969), Pogany & Turner (1968), Moodie (1972), Buxton *et al.* (1976), and Gunning & Goodman (1992).

Reciprocity represents a reverse-incidence configuration reached with the reversed wavevectors $\bar{\mathbf{k}}_0 = -\mathbf{k}_g$ and $\bar{\mathbf{k}}_g = -\mathbf{k}_0$, so that the scattering vector $\Delta\mathbf{k} = \mathbf{k}_g - \mathbf{k}_0 = \bar{\mathbf{k}}_0 - \bar{\mathbf{k}}_g$ is unchanged, but $\bar{\mathbf{K}}_{0g} = \frac{1}{2}(\bar{\mathbf{k}}_0 + \bar{\mathbf{k}}_g)$ is changed in sign and hence reversed (Moodie, 1972). The reciprocity equation,

$$\mathbf{u}_{g,\mathbf{K}} = \mathbf{u}^{*}_{g,\bar{\mathbf{K}}}, \tag{2.5.3.1}$$

is valid independently of crystal symmetry, but cannot contribute symmetry to the pattern unless a crystal-inverting symmetry element is present (since $\bar{\mathbf{K}}$ belongs to a reversed wavevector). The simplest case is centrosymmetry, which permits the right-hand side of (2.5.3.1) to be complex-conjugated giving the useful CBED pattern equation

$$\mathbf{u}_{g,\mathbf{K}} = \mathbf{u}_{\bar{g},\mathbf{K}}. \tag{2.5.3.2}$$

Since $\mathbf{K}$ is common to both sides there is a point-by-point identity between the related distributions, separated by $2g$ (the distance between g and $\bar{g}$ reflections). This invites an obvious analogy with *Friedel's law*, $F_g = F^{*}_{\bar{g}}$, with the reservation that (2.5.3.2) holds only for centrosymmetric crystals. This condition (2.5.3.2) constitutes what has become known as the $\pm H$ symmetry and, incidentally, is the only reciprocity-induced symmetry so general as to not depend upon a disc symmetry-point or line, nor on a particular zone axis (*i.e.* it is not a point symmetry but a translational symmetry of the pattern intensity).

2.5.3.2.3. *In-disc symmetries*

(*a*) *Dark-field (diffracted-beam) discs*. Other reciprocity-generated symmetries which are available for experimental observation relate to a single (zero-layer) disc and its origin $\mathbf{K}_g = \mathbf{0}$, and are summarized here by reference to Fig. 2.5.3.2, and given in operational detail in Table 2.5.3.2. The notation subscript R, for reciprocity-induced symmetries, introduced by Buxton *et al.* (1976) is now adopted (and referred to as BESR notation). Fig.

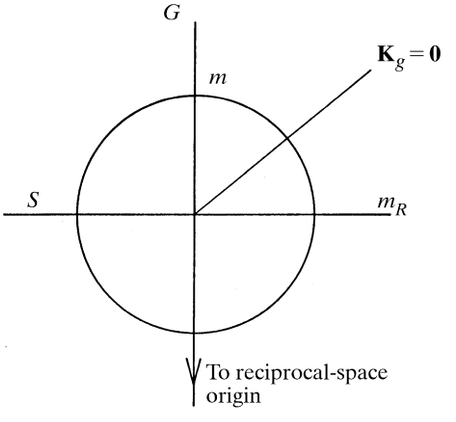

Fig. 2.5.3.2. Diagrammatic representation of a CBED disc with symmetry lines m, m_R (alternate labels G, S) and the central point $\mathbf{K}_g = 0$.

references